Inner limiting Membrane Peel Extends *In vivo* Calcium Imaging of Retinal Ganglion Cell Activity Beyond the Fovea in Non-Human Primate

Abbreviated Title: *Ca2+ imaging of retinal neurons beyond the fovea*

Hector C. Baez[1,2], Jennifer M. LaPorta[2], Amber D. Walker[2], William S. Fischer[2], Rachel Hollar[2,3], Sara Patterson[2], David A. DiLoreto Jr[2,3], Vamsi Gullapalli[3], Juliette E. McGregor[2,3]

1) Department of Biomedical Engineering, University of Rochester, Rochester, NY

2) Center for Visual Science, University of Rochester, Rochester, NY

3) Department of Ophthalmology, Flaum Eye Institute, University of Rochester Medical Center, Rochester, NY

Corresponding Author 1: Juliette E. McGregor jmcgrego@ur.rochester.edu

Corresponding Author 2: Hector Baez Hbaez@ur.rochester.edu

Keywords: GCaMP, AOSLO, RGC, ILM Peel, Calcium Imaging, In-vivo, retinal imaging

Number of pages: 42
Number of figures: 7
Number of Tables: 2

Number of multimedia: 1

Number of words for abstract: 244

Number of words for introduction: 544

Number of words for methods: 2184

Number of words for results: 1228

Number of words for figure legends: 815

Number of words for discussion: 1426

The authors declare no conflicts of interest

Acknowledgements

The authors would like to thank Qiang Yang and the Penn Vector Core (RRID: SCR_022432) at the Perelman School of Medicine, University of Pennsylvania. Research reported in this publication was supported by the National Eye Institute of the National Institutes of Health under Audacious Goals Initiative funding award No. U24 EY033275 Accelerating photoreceptor replacement therapy with in-vivo cellular imaging of retinal function, P30 EY001319 (core) and F32 EY032318 Foveal ganglion cell function in the living eye. The content is solely the responsibility of the authors and does not necessarily represent the official views of the National Inst. of Health. This study was supported by an Unrestricted Grant to the University of Rochester Department of Ophthalmology from Research to Prevent Blindness.

Abstract

Purpose: Adaptive Optics Scanning Light Ophthalmoscopy (AOSLO) paired with intravitreal injection of a viral vector coding for the calcium indicator GCaMP has enabled visualization of neuronal activity in retinal ganglion cells (RGCs) at single cell resolution in the living eye. However, the inner limiting membrane (ILM) restricts viral transduction to the fovea in humans and non-human primates (NHP), hindering both therapeutic intervention and physiological study of the retina. To address this, we explored peeling the ILM before intravitreal injection to expand calcium imaging beyond the fovea in the living primate eye.

Methods: Five eyes from Macaca fascicularis (age 3-10; n=3; 2 males, 1 female) underwent vitrectomy and ILM peel centered on the fovea prior to intravitreal delivery of 7m8:SNCG:GCaMP8s. RGC responses to visual flicker were evaluated using AOSLO calcium imaging 1-6 months post intravitreal injection.

Results: Calcium activity was observed in RGCs throughout the ILM peeled area in all eyes, representing a mean 8-fold increase in accessible recording area relative to a representative control eye. RGC responses in the ILM peeled and control eyes were comparable and showed no significant decrease over the 6 months following the procedure. In addition, we demonstrated that activity can be recorded directly from the retinal nerve fiber layer.

Conclusions: Peeling the ILM is a viable strategy to expand viral access to the GCL for gene therapies in NHP. Overall, this approach has potential to advance visual neuroscience, including pre-clinical evaluation of retinal function, detection of vision loss, and assessment of therapeutic interventions.

Introduction

The retina is a highly specialized tissue in the back of the eye that plays a critical role in the capture and processing of visual information. Advances in methods to study retinal function have enhanced our ability to understand retinal physiology, disease and to evaluate and optimize therapeutic interventions. In vivo measures of function allow us to gain insight into retinal activity in an intact tissue with the integrity of both circuitry and bodily systems maintained. This is particularly important for pre-clinical development where the immune system may be provoked by the intervention. In vivo recording of retinal function also enables indefinite longitudinal follow up. The non-human primate (NHP) is the gold standard animal model for both retinal physiological study and pre-clinical testing of novel therapies, owing to the close similarity between the visual and immune systems of humans. In vivo measures of function are therefore particularly appealing in NHP where numbers are few but the potential for translation is high.

70 The ideal *in vivo* functional testing paradigm would evaluate retinal activity at the cellular
71 scale throughout the retina. Multi-electrode array and patch clamp electrophysiology in retinal
72 explants are widely used and allow recordings with high temporal resolution, but rapid
73 degradation of the explant precludes longitudinal measurements in a single individual,
74 complicating assessment of pathologies or therapies particularly when the time course is
75 uncertain [1,2]. Electroretinography (ERG) enables repeated non-invasive measurement of retinal
76 responses in vivo [3,4], but does not read out activity at the cellular scale. Behavioral testing can
77 complement optical and electrophysiological [5], but does not provide direct insight into function at
78 the retinal level or at the cellular scale.

79 By pairing adaptive optics scanning laser ophthalmoscopy (AOSLO) which enables high
80 resolution retinal imaging [6] with viral vector mediated expression of the genetically encoded
81 calcium indicator GCaMP, it is now possible to optically read out RGC activity at the cellular scale
82 in NHP *in vivo* [7-9]. However, viral transduction of RGCs following intravitreal injection of an AAV
83 has previously been spatially restricted to a ring of RGCs serving the most central foveal cones
84 in primates [10] as the inner limiting membrane (ILM), a thin border between the retina and vitreous
85 fluid formed by astrocytes and end feet of Müller cells, creates a barrier to viral penetration
86 outside of the foveal pit [11]. Peeling the ILM prior to intravitreal injection has reliably expanded
87 viral transduction of GFP in retinal neurons [12-14] and this approach has been proposed as a
88 strategy to dramatically expand the area of RGCs transduced by gene therapies.

89 In this study we dramatically expand the area of the NHP retina accessible for optical
90 recording of function in vivo by removing the ILM prior to intravitreal injection of the viral vector
91 coding for GCaMP. Not only does this expand the potential utility of this optical recording platform
92 in vivo but it also provides insight into the impact of the ILM procedure on the retina at the cellular
93 scale in the living eye. We obtain RGC responses at eccentricities that were previously
94 inaccessible in multiple animals and present the first optical recordings from the retinal nerve

fiber layer (RNFL). Longitudinal calcium imaging AOSLO is performed to together with OCT and fundus photography to better understand outcomes associated with the ILM peel procedure.

Materials and Methods

Experimental Design

Five experimental eyes and one control eye from 3 Macaca fascicularis (2 male, one female) were used in this study. All five experimental eyes were vitrectomized and underwent peeling of the ILM centered on the fovea (Figure 1A-B). Six to eight weeks later, intravitreal injection of a viral vector was performed to produce GCaMP expression in the ganglion cell layer (Figure 1C). Three of the five experimental eyes received intravitreal injection of viral vector AAV2.7m8-SNCG-GCaMP8s while the two eyes of macaque M3 received the GCaMP8m variant. One control eye did not undergo vitrectomy or ILM peeling (Table 1). We did not perform a vitrectomy without ILM peel as an additional control because previous studies have established that vitrectomy alone insufficient to extend viral transduction [12].Scanning laser ophthalmoscopy (cSLO) confirmed the presence of GCaMP in the area corresponding to region of ILM peeling surgical peel (Figure 1D). cSLO, OCT, and color fundus photography were performed longitudinally up to six months post procedure. Functional assessment at the cellular scale *in vivo* was conducted using fluorescence AOSLO in combination with a red LED flashing stimulus (Figure 1E-G). Retinal imaging was conducted between the fovea and the ILM peel edge in all meridians.

Animal welfare

117 The macaques used in this study were housed in pairs in an AAALAC accredited facility in
118 compliance with the University of Rochester University Committee on Animal Resources (UCAR).
119 They had free access to water and primate biscuits, providing a complete and nutritious diet. To
120 supplement this, they were given various treats multiple times daily, such as nuts, dried fruit,
121 vitamin chews, and a large variety of fresh fruits and vegetables. They were also given "high
122 value" treats during training, including Ensure, marshmallow snacks, and fruit gummies. An
123 animal behaviorist and Veterinary Technicians provided novel enrichment items multiple times a
124 week, including items such as grass, oranges with peels still on, treat filled forage boxes,
125 grapevines, water play, and popcorn balls. Daily enrichment included mirrors, puzzle feeders,
126 durable chew toys, daily television time and/or music and regular visits from staff to offer treats
127 and socialization. All macaques were cared for by the Department of Comparative Medicine
128 veterinary staff, including three full-time Veterinarians, five Veterinary Technicians, and an animal
129 care staff who monitored animal health and comfort at least three times daily. The Animal
130 Behaviorist regularly recorded and analyzed primate behavior to monitor any signs of stress. This
131 study was carried out in strict accordance with the Association for Research in Vision and
132 Ophthalmoscopy (ARVO) Statement for the Use of Animals and the recommendations in the
133 Guide for the Care and Use of Laboratory Animals of the National Institutes of Health. The
134 protocol was approved by the University Committee on Animal Resources of the University of
135 Rochester (PHS assurance number: D16-00188(A3292-01)).

136

137 **Immunosuppression**

138 All macaques in this experiment received subcutaneous Cyclosporine injections daily. Blood
139 trough levels were collected to titrate the dose of 150-250 ng/mL and then maintained at that

140 level. The timing of immune suppression relative to ILM peel surgery and viral vector injections
141 are detailed in Table 1.

142

143 **Animal preparation for ILM peel surgery**

144 The surgical subject was fasted overnight with free access to water. The animal was sedated
145 using ketamine (100mg/mL) and medetomidine (20mg/mL), then intubated and kept at proper
146 anesthetic depth via 1.5-3% isoflurane throughout the procedure. The animal was positioned in
147 dorsal recumbency on a padded surgical table. A Bair Hugger warming system was placed over
148 the animal to maintain body temperature. Vital signs including temperature, heart rate and
149 rhythm, respirations, end tidal CO_2, blood pressure, SpO_2, and reflexes were monitored
150 consistently and recorded every fifteen minutes. Pupil dilation was accomplished using 1%
151 atropine ophthalmic solution. An aseptic preparation was performed on the surgical eye and
152 surrounding area using 5% betadine solution and flushed with sterile 0.9% saline. The subject's
153 eye and body were then draped in a sterile fashion.

154

155 **ILM Peel procedure**

156 The ILM peel procedures performed in NHP closely followed the protocol used in human surgery.
157 A standard 3-port pars plana vitrectomy was performed through 25-gauge cannulas using the
158 Constellation vitrectomy system (Alcon, Ft. Worth, TX), OPMI Lumera 700 operating microscope,
159 and RESIGHT viewing system (Carl Zeiss Meditec AG, Jena, Germany). Triamcinolone was
160 injected intravitreally to visualize the vitreous. A posterior vitreous detachment was induced using
161 aspiration from the vitrector or a soft tip cannula. The peripheral vitreous was trimmed. Brilliant
162 Blue G Ophthalmic Solution (DORC) dye was placed over the macula and the ILM stained for 2
163 minutes (Supplementary Movie 1). A fluid-fluid exchange was performed to remove the dye. The

164 stained ILM was then peeled 360 degrees, centered on the fovea, in approximately 5 to 6-disc
165 diameter area in the macula using ILM peeling forceps (Alcon, Ft. Worth, TX) (Supplementary
166 Movie 2). The three ports were then removed at the end of the surgery and the sclerotomies
167 sutured. The animal was given an intravitreal injection of vancomycin (1mg/0.1mL) and
168 ceftazidime (2mg/0.1mL). Immunosuppressant Cyclosporine (150-250ng/mL), anti-inflammatory
169 meloxicam (5mg/mL), analgesic buprenorphine SR (3mg/mL), and an anesthetic reversal of
170 antisedan (5mg/mL) were all administered post-operatively.

171

172 **Intravitreal Injection of viral vector**

173 Intravitreal injection of AAV2-7m8.SNCG.jGCaMP8s.WPRE.SV40 (100 μL at titer 2.62×10^{13}
174 GC/mL), or AAV2-7m8.SNCG.jGCaMP8m.WPRE.SV40 (100 μL at titer ≥ 2.46×10^{13} GC/mL),
175 was performed as previously described in Yin et al 2011 [15]. Briefly, the eye was sterilized with 5%
176 diluted betadine before the vector was injected into the vitreous through the pars plana using a
177 tuberculin syringe and 30-gauge needle. All viral vectors were synthesized by the University of
178 Pennsylvania Vector Core. Neutralizing antibodies to AAV2 were 1:25 or lower in all four injected
179 animals prior to the study. Following the intravitreal injection of the vector, each eye was imaged
180 weekly with a conventional scanning light ophthalmoscope (Heidelberg Spectralis, Heidelberg
181 Engineering, Franklin, MA) using the 488 nm autofluorescence modality, to determine the onset
182 of expression, image quality and to monitor eye health. The animal received 2mg/0.05mL of
183 triamcinolone intravitreally (Kenalog-40) following the injection to treat for symptoms of uveitis.

184

185 **Animal preparation for imaging**

All monkeys were fasted from 4 to 18 h prior to anesthesia induction. Anesthesia induction began with 5 to 20 mg/kg Ketamine, 0.25 mg/kg Midazolam, and 0.017 mg/kg Glycopyrrolate intramuscularly. The pupil was dilated with a combination of tropicamide 1% and phenylephrine 2.5%. In cases of minimal pupil dilation within the standard time, phenylephrine 10% and/or cyclopentolate 1% drops were administered. Flurbiprofen Ophthalmic drops are given to the target eye, to prevent any discomfort from prolonged use of an eye lid speculum. Both eyes were covered with a hydrating ophthalmic gel (GenTeal). The target eye then had the lid speculum placed to keep the eye open during imaging and a contact lens was placed to ensure corneal protection. The fellow eye was taped closed with porous tape, to protect the cornea from drying.

The animal was placed in a stereotaxic cart. Prior to intubation, an oxygen mask with 1–2% isoflurane, was placed over the monkey's face to allow for adequate sedation for intubation. An intravenous drip of Ringer's lactate with 5% dextrose was maintained at 5 ml/kg/hr for the duration of imaging. The monkey was intubated and maintained at a surgical plane of anesthesia with isoflurane 1.0–2.5%. A Bair Hugger warming system was placed over the monkey to maintain body temperature. Monitoring was conducted as previously described.

After a surgical plane of anesthesia had been established, a Rocuronium infusion (800mcg/ml) was given with a dose range from 200-600mcg/kg/hr, after an initial bolus dose of 100-400mcg/kg. Rocuronium is administered to effect, determined by eye movement, and the lowest effective dose per animal is used. Once respirations ceased, the monkey was maintained on a ventilator until imaging was over and the infusion was turned off. Once a peripheral nerve response was established, an intravenous dose of glycopyrrolate 0.01 mg/kg was given. Five minutes after the glycopyrrolate, neostigmine 0.05 mg/kg was given intravenously. The monkey was monitored for indications of breathing against the ventilator and then removed from the ventilator once able to breath without assistance. The monkey was removed from the isoflurane

no sooner than fifteen minutes after the neostigmine injection to ensure stability off the ventilator. The monkey was then allowed to wake up and extubated once all reflexes had returned.

Clinical imaging

Confocal scanning light ophthalmoscopy (cSLO), optical coherence tomography (OCT) and color fundus photography were performed to pre- and post-procedure using a commercially available Spectralis HRA (Heidelberg Engineering) and fundus camera (Topcon 50EX). The blue autofluorescence modality on the spectralis HRA was used to capture GCaMP fluorescence using the 488nm excitation wavelength and a longpass filter at 500nm. GCaMP fluorescence was also captured using the fundus camera equipped with filters selective for GCaMP excitation and emission (ex. 472/30 nm em. 520/28 nm). 30- and 55-degree OCT images centered on the fovea were collected pre- and post-ILM peel, pre-and post-intravitreal injection, and roughly every 30 days thereafter. OCT data from the optic nerve head in addition to slit lamp photographs (Zeiss) were recorded at the same timepoints to document the time course and severity of any inflammation.

Assessing ocular inflammation

A modified Hackett-McDonald scoring system [16] was used to evaluate ocular inflammation. A Veterinary technician evaluated the pupil reflex and conjunctival discharge prior to pupil dilation. A comprehensive set of slit lamp images were recorded, randomized and graded by an ophthalmologist (VG). The scoring system is available in the supplementary materials.

Calcium Imaging Adaptive Optics Scanning Laser Ophthalmoscopy

AOSLO data were collected using a previously described AOSLO instrument [17,18]. An 847nm diode laser (QPhotonics, 100-136uW/mm2) was used as a wavefront sensing beacon in combination with a Shack-Hartman wavefront sensor and a deformable mirror (ALPAO) for measuring and correcting the optical aberrations of the eye. A 796nm superluminescent diode (Superlum, 700-850uW/mm^2) was used to image the cone photoreceptor layer using a 2 airy disc (20um) pinhole to collect the reflected light. Simultaneously, a 488nm laser (Qioptiq, 57uW/mm2) focused on the RGC layer was used to excite GCaMP and emitted fluorescence was collected using a 7.5 airy disc (75um) pinhole. Laser powers were calibrated prior to every imaging session to ensure consistency across sessions. To correct for longitudinal chromatic aberration between the 796nm source and 488nm sources on the detector, motorized stages were adjusted to optimize their positions *in vivo* prior to each experiment. The adaptive optics control facilitated fine focus on the retinal ganglion layer of the 2.54° by 2.54° field of view at each retinal location. GCaMP fluorescence (emission 535/20 nm) was recorded in response to 7 degree uniform visual stimulus presented through a Maxwellian view system [19]. A Thorlabs mounted LED with a 661/20 nm emission filter was used as the visual stimulus to avoid the GCaMP excitation spectrum and consisted of 20 second contrast increments and decrements against a mean light level (3 μW/mm^2). Trials began with a 60 second system background period with no laser emission, this was followed by a 120 second light adaptation period to the 488nm imaging laser and the mean luminance of the visual stimulus before 20 second increments and decrements began. Fluorescence was recorded during the system background, period of constant illumination and the stimulation period. Each trial was repeated twice at each retinal location. Total exposure to all laser sources was kept below the Rochester exposure limit [20], designed to be two-fold more conservative than the ANSI standard [21].

Data Analysis

Adaptive optics calcium imaging was stored as an uncompressed AVI video format. A frame-by-frame stimulus information was written to a csv file, providing an accurate record for analysis. The reflectance videos of the photoreceptor mosaic were registered offline using a strip-based cross correlation algorithm [22], that corrected translational motion between frames and intraframe warping due retinal motion. Each frame of the GCaMP fluorescence video was co-registered to the photoreceptor reflectance video. The frames of the fluorescence video were temporally integrated to form a high SNR z projection image that was used to create an RGC segmentation mask using FIJI. RGC segmentation masks were then imported into MATLAB and used to tabulate individual cell traces for each imaging location. These cell traces were then filtered using a 50-frame moving median filter. The Z-score was calculated as the GCaMP response amplitude (signal) minus the mean amplitude of the baseline adapted response (noise), all divided by the standard deviation of the noise. The criterion for a responsive cell was set to 2.5 standard deviations above the noise. Statistical analyses were performed using MATLAB two-sample T-test, with group spread reported as mean ± SD. Fluorescence cSLO images were scaled and manually segmented using FIJI to determine the boundaries of GCaMP expression.

Following RGC imaging, we recorded from the RNFL near the optic disc in the same sessions. We used the same imaging and stimulation paradigm to collect this data with the expectation that the 7-degree uniform visual stimulus would excite ganglion cells within the area of GCaMP expression. We integrate a large area encompassing multiple passing fibers to enable extraction of population-level responses.

Code and Data Accessibility

All code used for analysis and corresponding filtered RGC recordings will be made available on our GitHub and the open science framework repository upon publication. Raw video data is available upon request.

Results

ILM peel enables functional recording from RGCs at previously inaccessible eccentricities *in vivo*

To assess the impact of ILM peel on the spatial extent of GCaMP transduction in the GCL we directly compared the pattern of expression in the ILM peeled eye with the fellow eye of the same animal (M1), which received an intravitreal injection but no ILM peel (control). Figs 2A and 2B show a dramatic 5-fold increase in the area of GCaMP expressing RGCs in the ILM peeled eye (12.9 mm^2) relative to the control (2.5 mm^2). In the ILM peeled eye, RGCs were transduced with GCaMP out to 9.2 degrees superior to the fovea whereas in the control eye the maximum eccentricity was just 3.5 degrees. The increased fluorescence relative to the autofluorescent background observed in Figure 2B extended to the limit of the ILM peel identified by retinal landmarks in the surgical video. Furthermore, imaging with a fluorescence fundus camera equipped with filters selective for GCaMP excitation and emission confirmed that the elevated fluorescence was the extrinsic fluorophore GCaMP.

To assess the responses of RGCs in the ILM peeled and control eye we performed calcium imaging AOSLO while the retina received periodic visual stimulation at 0.025Hz. Figure 1G shows an example fluorescence trace from a single ON cell in the ILM peeled eye. The magnitudes of single cell responses recorded in the ILM peeled and control eyes are shown in Figure 2C, represented as z-scores. The distribution of z-scores from individual RGCs in the ILM

peeled and control eyes were not significantly different at 1° (P=0.07) or 3.5° (P=0.61), suggesting that the ILM peel did not adversely impact RGC physiology. Importantly only in the ILM peeled eye was it possible to obtain functional recording from RGCs at eccentricities beyond 3.5 degrees. Figure 2C shows responses collected from RGCs at 9.2 degrees from the foveal center. This is the first-time *in vivo* calcium imaging has been performed outside the parafovea. No RGCs fluoresced beyond four degrees from the fovea in M1 OS. Z-scores from M1 OD at 9.2 degrees were found to be significantly lower than those at 3.5 degrees in the same eye (P=0.0004).

As functional recordings were obtained *in vivo,* it was possible to return to the same region of the GCL to longitudinally monitor RGC responses over a period of months (Figure 3). For M1 OD, RGC response amplitudes at 9 degrees did not significantly change over time (Figure 3A-B; paired t test; P=0.86, P=0.42), but the amplitudes at 3 degrees significantly increased after 5 months (Figure 3C-D; paired t test; P=0.02). Compared to the non-ILM peeled fellow eye at 3.5 degrees (Figure 3E-F) that was injected first, OD had significantly higher amplitudes (paired t test; p=0.021). While responses varied week to week, no long-term decline in the calcium responses of RGCs were observed, suggesting that RGC function was not significantly compromised by the ILM peel procedure.

To assess the reproducibility of this approach an additional 4 eyes underwent ILM peeling prior to intravitreal injection of the viral vector and follow up imaging. Across all eyes we observed an average 8-fold increase in area (12.9mm^2, 24.4 mm^2, 20.1 mm^2,22.7 mm^2, 20.7 mm^2, respectively) of GCaMP expression across all eyes relative to the control eye (2.5mm^2) as measured using BAF cSLO (Figure 4). We extracted functional activity from RGCs in all eyes at eccentricities out to 9.2, 7.4, 7.9, 11, and 6.2 degrees respectively. There was a significant decrease in response magnitude with eccentricity in M1 OD (p=0.0003) but not in M2 OS

327 (p=0.598), M2 OD (p=0.147), M3 OS (p=0.055), and M3 OD (p=0.122). We note that M2 had
328 naturally occurring vessel tortuosity.

329

330 **Optical readout of RGC activity is possible from the retinal nerve fiber layer**

331 For the first time we show that it is possible to record not only from RGC somas but also
332 from the RNFL near the optic disc (Figure 5). We evaluated calcium responses from the RNFL in
333 both the ILM peeled and control eye. The investigated locations were outside of the ILM peeled
334 area and as a result lacked fluorescing RGC somas but contained GCaMP expressing axonal
335 fibers (Figures A,C). The averaged signal from the integrated region (Figures 5B,D)
336 corresponded to an 'OFF' type response in both cases, but in the control eye the magnitude of
337 the response was reduced by half (3.3 ± 0.02, and 1.4 ± 0.02 Z-score, respectively) (Figure 6E).
338 In a representative location with both soma and RNFL, the RGC somas were more response
339 than segmented RNFL bundles (10.9 ± 7.63 and 5.28 ± 3.3 Z-score, respectively) with 400-fold
340 greater average pixel brightness.

341

342 **Structural imaging reveals minor morphological changes following ILM peel**

343 To ensure we had a full understanding of any structural changes in the retina resulting
344 from the ILM peel, we closely monitored all eyes over time with fundus photography and OCT
345 (Figure 6). Alteration of the foveal contour was visible in the B-scan OCT images of all subjects,
346 with the extent of this alteration varying between individuals. The foveal pit diameter of M1 OD
347 (Figure 6A) and M3 OD (Figure 6E) appears slightly reduced compared to pre-ILM peel, while,
348 the foveal contours of M2 (Figure 6B-C) and M3 OS (Figure 6D) are more dramatically altered.
349 These changes in foveal contour persist throughout the observation period (6 months post ILM

350 peel). No macular holes were created, but disruption to the photoreceptor layer was noted in M2
351 OS and improved over time.

352 Concentric macular dark spots (CMDS) [23], surrounding the fovea and aligned with the
353 sweep of retinal nerve fibers toward the optic disc were observed in the color fundus images of 3
354 of the 5 eyes (Figures 6B,C,D, white arrows). Shallow dimples in the RNFL were observed post
355 ILM peel in OCT-B scan data from all animals, consistent with previous reports of disassociated
356 optic nerve fiber layer (DONFL) [24,25].

357 To further investigate potential damage to the GCL or RNFL, we used high resolution
358 imaging to investigate retinal locations containing both darkened spots in color fundus (Figure
359 7B,D,F) and DONFL in the OCT-B scan. Our findings confirmed for the first time that dimples
360 present in the RNFL correlated to the absence of small (< 100um) pockets of RGCs (Figure
361 7A,C,E). This RGC loss was variable between animals. Animal M3 OS (Figure 7D, left panel) had
362 only one hypofluorescent region near the edge of expression (Figure 7D, right panel) while other
363 eyes had them close to the fovea predominantly in temporal retina. To test the connection
364 between CMDS and the RNFL dimples in OCT we investigated patches of CMDS with high
365 resolution imaging, finding that these were not associated with missing RGCs. As one example,
366 in M3 OS (Figure 7F-G) the DONFL region does not appear on the OCT as a dimple in the RNFL
367 nor in the AOSLO modality as hypofluorescent.

368 A board-certified ophthalmologist evaluated ocular inflammation for 4 eyes of 2 animals
369 following intravitreal injection of the viral vector based on a modified Hackett-McDonald scoring
370 system (Table 2) [29]. In M2, inflammation was characterized principally by conjunctival
371 congestion, swelling, and decreased corneal transparency with pigment noted on the anterior
372 capsule of OS up to 12 weeks post injection. M3 primarily experienced decreased corneal

transparency along with minor conjunctival congestion and swelling up to 7 weeks post injection. Despite temporary inflammation, GcAMP was present in all eyes for the duration of this study.

Discussion

Surgical removal of the ILM prior to intravitreal injection of a viral vector coding for GCaMP enabled a mean 8-fold expansion of the area of the retina accessible for optical recording from RGCs across the 5 primates tested in this study. These are the first optical measurements at eccentricities beyond a small (< 3 degree) foveal ring that have been achieved *in vivo* and the first demonstration that optical recording from the RNFL is possible. Longitudinal recordings of RGC calcium responses over weeks and months showed variation but no significant long-term decline, suggesting that RGC function was not significantly compromised by the ILM peel procedure. This result is promising for future applications of ILM peeling in gene and cell therapies. In addition, we used AOSLO to investigate previously reported structural defects associated with the ILM peel procedure and observed a variable number of small hypo fluorescent regions of RGC loss, more common in temporal retina and visible as depressions in the OCT images of the GCL. This minimal loss of discrete patches of RGCs may be an acceptable tradeoff given the expanded region accessible for calcium imaging *in vivo* or for therapeutic applications.

The advances presented in this paper have implications for both retinal neuroscience, pre-clinical assessment of retinal function, and for the delivery of new therapies that could utilize the ILM peel procedure. The ability to functionally survey large areas of the GCL beyond the fovea both in vivo and at the cellular scale could be valuable in identifying and interrogating rare classes of primate RGCs and understanding how these cells change with eccentricity. From a pre-clinical standpoint, the cellular scale assessment of retinal function in vivo has potential to

397 advance our ability to characterize disease models and detect and track restored RGC function
398 that might be spatially and temporally sporadic, for example in the development of cell therapies.
399 In this use case, peeling the ILM would expand the available surface area for therapeutic
400 investigation 8-fold. Lastly surgical peel of the ILM may be a viable strategy to expand region of
401 the retina that can be transduced by gene therapies or receive RGC transplants. The results
402 presented here suggest that RGC function is not severely impacted by this intervention in the
403 months after surgery and in the case of e.g. optogenetic gene therapy targeting RGCs, ILM peel
404 could substantially increase the patients restored visual angle and any potential benefit derived
405 from this therapy.

406

407 **Variability in RGC responses between subjects**

408 We observed a substantial variability in Z scores between animals, with subject M1
409 responding with significantly higher z-scores relative to other experimental eyes. A variety of
410 factors could be behind this, but we note that M1 was significantly older (10 as opposed to 4
411 years) and had fewer inactivating antibodies to AAV2 (Table 1). Age can have an impact on
412 innate immunity, and could have affected the efficacy of viral transduction or the degree of
413 inflammation impacting anterior segment optics. M1 also had a much shorter time between ILM
414 peel and the first intravitreal injection, minimizing any potential obstruction of viral access to the
415 GCL by glia mediated scar formation, as while the ILM does not regrow, Muller glia produce a
416 basement membrane that covers most of the exposed retina [26].

417

418 **Functional responses were obtained from the RNFL**

419 We were able to extract functional assessment of responses carried along RGC axons in
420 addition to those recorded directly from RGC somas. This was possible both in the control eye

421 and the ILM peeled eye, but with double the Z score in ILM peeled eyes relative to the control
422 (figure 4). This could be explained by the increased number of GCaMP-expressing RGCs in the
423 ILM peeled eye and therefore a larger number of GCaMP expressing axons traversing the field of
424 view. We note that the RNFL trace was dominated by an OFF response that may be explained by
425 the stimulus design. A high photopic mean light level can drive stronger OFF responses than ON.
426 An enlarged, pan retinal stimulus could further increase the measured RNFL response by
427 activating additional RGCs. This finding raises the possibility of RGC responses being
428 contaminated by the overlying RNFL. The Z score per pixel is X fold higher in cell somas relative
429 to the RNFL and soma signals therefore dominate in standard recordings but it is important to
430 note that these effects may more visible in deafferented retina. For this same reason, RGC
431 somas make it difficult to extract signals from the RNFL unless recordings are made beyond the
432 edge of the ILM peel. Recording directly from the RNFL may be of interest in pre-clinical models
433 of glaucoma or assessing axon regeneration of transplanted ganglion cells *in vivo* [27]. Future work
434 may focus on segmenting responses from individual axon bundles to better understand
435 organization of functional responses traveling to the optic disc.

436

437 **The ocular inflammation associated with viral vector injections in immune suppressed,**
438 **ILM peeled animals does not prevent functional recording**

439 Inflammation was observed in the weeks following viral vector injection in the eyes scored
440 in this study (Table 1). The duration and extent of inflammation varied between immune
441 suppressed animals but we did not observe a substantial increase in inflammation relative to a
442 previous report from a non-vitrectomized, non-ILM peeled primate eye intravitreally injected with
443 vector AAV2:CAG:GCaMP6s [28]. Relative to this animal, M2 scored higher in overall inflammatory
444 response while M3 scored lower with both M2 and M3 recovering faster. The present study used

445 a ganglion cell specific promoter SNCG [29] instead of the ubiquitous promoter CAG, a different
446 serotype (7m8 instead of AAV2) and GCaMP generation (GCaMP8 instead of GCaMP6) than the
447 previous study, making a direct comparison challenging, but the general similarities suggest that
448 inflammation does not preclude adoption of this technique in a pre-clinical context.

449

450 **Surgical outcomes associated with peeling the ILM**

451 This study demonstrates the feasibility of using an ILM peel to expand the imaging area for
452 functional assessment of macaque RGCs, but also provides new insight into outcomes
453 associated with the surgery itself. Consistent with clinical literature, the most obvious
454 consequence of ILM peel is an altered foveal contour (Figure 6) consistent with previously
455 reported increase in central macular thickness [30]. CMDS and DONFL were also observed, the
456 latter being associated with small pockets of RGC loss and occurring more frequently in temporal
457 retina where the RNFL is thinner [31]. This result is consistent with immunohistochemical studies of
458 excised ILM, suggesting that RGCs are removed during the ILM peel process [32] but these had
459 not previously been visualized at the cellular scale in vivo. Limited pockets of ganglion cell loss
460 may be tolerable given the increases in the recording area, particularly as their locations are
461 clear.

462 **Alternatives to ILM peeling**

463 Alternative methods to circumvent the restricted viral transduction imposed by the ILM in
464 primates have been suggested including enzymatic digestion of the ILM with a nonspecific
465 protease [11,33], photodisruption [34,35] or sub-ILM injection [36]. Enzymatic digestion has the advantage
466 of not requiring surgery, but has not been attempted in NHPs, where the ILM is thicker than in
467 small animal models. As ILM thickness is eccentricity dependent in primates, it is not
468 straightforward to titrate the correct dose, risking substantial retinal damage. Photodisruption of

469 the ILM has been tested successfully in bovine retinal explants [34] using indocyanine green and
470 recently this work has been extended to an *in vivo* rabbit model [37], but further testing is
471 necessary before it can be applied to NHP. Lastly an alternative surgical strategy is sub-ILM
472 delivery of the viral vector which may yield similar results while keeping more of the structure
473 intact. As the ILM is composed of Muller cell foot plates, its removal has the potential to cause
474 Muller cell dysfunction [38]. ILM delivery is therefore desirable, but is surgically very challenging
475 given the thickness of the ILM and there is a risk of delivering the viral vector sub-retinally or sub-
476 hyloid, neither of which would target the GCL.

477 **Conclusions**

478 This study demonstrates not only that the ILM peel approach allows functional recording
479 from a larger area of the GCL but also that the recordings remain stable over time and are
480 comparable to those in eyes with no ILM peel. As such, this technique may be of value for pre-
481 clinical evaluation of retinal function, both for detecting vision loss and assessing the impact of
482 therapeutic interventions. For cell-based therapies where single cell resolution is needed, a
483 larger area to assess retinal function would greatly increase the chance of success given the
484 potential sparse integration and uncertainty of the locus of cell delivery.

485

486 **References**

487 1. Gauvain G, Akolkar H, Chaffiol A, et al. Optogenetic therapy: high spatiotemporal resolution and
488 pattern discrimination compatible with vision restoration in non-human primates. *Commun Biol*.
489 Jan 27 2021;4(1)doi:ARTN 125

490 10.1038/s42003-020-01594-w
491 2. Ganjawala TH, Lu Q, Fenner MD, Abrams GW, Pan ZH. Improved CoChR Variants Restore Visual
492 Acuity and Contrast Sensitivity in a Mouse Model of Blindness under Ambient Light Conditions.
493 *Molecular Therapy*. Jun 5 2019;27(6):1195-1205. doi:10.1016/j.ymthe.2019.04.002
494 3. Le Meur G, Stieger K, Smith AJ, et al. Restoration of vision in RPE65-deficient Briard dogs using an
495 AAV serotype 4 vector that specifically targets the retinal pigmented epithelium. *Gene Ther*.
496 2007/02/01 2007;14(4):292-303. doi:10.1038/sj.gt.3302861

4. Pearson RA, Barber AC, Rizzi M, et al. Restoration of vision after transplantation of photoreceptors. *Nature*. 2012/05/01 2012;485(7396):99-103. doi:10.1038/nature10997
5. Nikonov S, Aravand P, Lyubarsky A, et al. Restoration of Vision and Retinal Responses After Adeno-Associated Virus-Mediated Optogenetic Therapy in Blind Dogs. *Transl Vis Sci Techn*. May 2022;11(5)doi:ARTN 24

10.1167/tvst.11.5.24
6. Roorda A, Romero-Borja F, Donnelly WJ, Queener H, Hebert TJ, Campbell MCW. Adaptive optics scanning laser ophthalmoscopy. *Opt Express*. May 6 2002;10(9):405-412. doi:10.1364/Oe.10.000405
7. McGregor JE, Godat T, Dhakal KR, et al. Optogenetic restoration of retinal ganglion cell activity in the living primate. *Nat Commun*. Apr 3 2020;11(1):1703. doi:10.1038/s41467-020-15317-6
8. McGregor JE, Yin L, Yang Q, et al. Functional architecture of the foveola revealed in the living primate. *PLoS One*. 2018;13(11):e0207102. doi:10.1371/journal.pone.0207102
9. Yin L, Masella B, Dalkara D, et al. Imaging Light Responses of Foveal Ganglion Cells in the Living Macaque Eye. *The Journal of Neuroscience*. 2014;34(19):6596-6605. doi:10.1523/jneurosci.4438-13.2014
10. Comander J, Carvalho LS, Xiao R, et al. Characterization of the limitations to gene transfer and associated inflammation following intravitreal AAV injection in nonhuman primates. *Investigative Ophthalmology & Visual Science*. 2016;57(12):771-771.
11. Dalkara D, Kolstad KD, Caporale N, et al. Inner limiting membrane barriers to AAV-mediated retinal transduction from the vitreous. *Mol Ther*. Dec 2009;17(12):2096-2102. doi:10.1038/mt.2009.181
12. Takahashi K, Igarashi T, Miyake K, et al. Improved Intravitreal AAV-Mediated Inner Retinal Gene Transduction after Surgical Internal Limiting Membrane Peeling in Cynomolgus Monkeys. *Molecular Therapy*. 2017/01/04/ 2017;25(1):296-302. doi:https://doi.org/10.1016/j.ymthe.2016.10.008
13. Teo K, Lee SY, Constable I. The effect of Surgical removal of the Internal Limiting Membrane on AAV vector delivery to the Retina in a Non-Human Primate model. *Investigative Ophthalmology & Visual Science*. 2018;59(9):5660-5660.
14. Teo KYC, Lee SY, Barathi AV, Tun SBB, Tan L, Constable IJ. Surgical Removal of Internal Limiting Membrane and Layering of AAV Vector on the Retina Under Air Enhances Gene Transfection in a Nonhuman Primate. *Investigative Ophthalmology & Visual Science*. 2018;59(8):3574-3583. doi:10.1167/iovs.18-24333
15. Yin L, Greenberg K, Hunter JJ, et al. Intravitreal Injection of AAV2 Transduces Macaque Inner Retina. *Investigative Ophthalmology & Visual Science*. Apr 2011;52(5):2775-2783. doi:10.1167/iovs.10-6250
16. Munger RJ. Veterinary ophthalmology in laboratory animal studies. *Vet Ophthalmol*. Sep 2002;5(3):167-175. doi:10.1046/j.1463-5224.2002.00243.x
17. Gray DC, Merigan W, Wolfing JI, et al. In vivo fluorescence imaging of primate retinal ganglion cells and retinal pigment epithelial cells. *Opt Express*. Aug 7 2006;14(16):7144-7158. doi:10.1364/oe.14.007144
18. Godat T, Cottaris NP, Patterson S, et al. In vivo chromatic and spatial tuning of foveolar retinal ganglion cells in Macaca fascicularis. *PLoS One*. 2022;17(11):e0278261. doi:10.1371/journal.pone.0278261
19. Baron WS. Maxwellian view stimulator for electrophysiological or psychophysical work. *Appl Opt*. Nov 1 1973;12(11):2560-2562. doi:10.1364/AO.12.002560

20. Rossi EA, Rangel-Fonseca P, Parkins K, et al. In vivo imaging of retinal pigment epithelium cells in age related macular degeneration. *Biomed Opt Express*. 2013;4(11):2527-2539. doi:10.1364/BOE.4.002527
21. Thomas RJ, Rockwell BA, Marshall WJ, et al. Procedure for the computation of hazards from diffusely scattering surfaces under the Z136.1-2000 American National Standard for Safe Use of Lasers. *J Laser Appl*. Feb 2007;19(1):46-54. doi:Doi 10.2351/1.2402516
22. Yang Q, Zhang J, Nozato K, et al. Closed-loop optical stabilization and digital image registration in adaptive optics scanning light ophthalmoscopy. *Biomed Opt Express*. Sep 1 2014;5(9):3174-3191. doi:10.1364/BOE.5.003174
23. Alkabes M, Salinas C, Vitale L, Bures-Jelstrup A, Nucci P, Mateo C. En face optical coherence tomography of inner retinal defects after internal limiting membrane peeling for idiopathic macular hole. *Invest Ophthalmol Vis Sci*. Oct 21 2011;52(11):8349-8355. doi:10.1167/iovs.11-8043
24. Tadayoni R, Paques M, Massin P, Mouki-Benani S, Mikol J, Gaudric A. Dissociated optic nerve fiber layer appearance of the fundus after idiopathic epiretinal membrane removal. *Ophthalmology*. Dec 2001;108(12):2279-2283. doi:10.1016/s0161-6420(01)00856-9
25. Christensen UC, Kroyer K, Sander B, et al. Value of internal limiting membrane peeling in surgery for idiopathic macular hole stage 2 and 3: a randomised clinical trial. *Brit J Ophthalmol*. Aug 2009;93(8):1005-1015. doi:10.1136/bjo.2008.151266
26. Hisatomi T, Notomi S, Tachibana T, et al. Ultrastructural changes of the vitreoretinal interface during long-term follow-up after removal of the internal limiting membrane. *Am J Ophthalmol*. Sep 2014;158(3):550-556.e551. doi:10.1016/j.ajo.2014.05.022
27. de Lima S. Full-length axon regeneration in the adult mouse optic nerve and partial recovery of simple visual behaviors (vol 109, pg 9149, 2012). *P Natl Acad Sci USA*. Aug 14 2012;109(33):13465-13465. doi:10.1073/pnas.1211885109
28. McGregor JE, Kunala K, Xu Z, et al. Optogenetic therapy restores retinal activity in primate for at least a year following photoreceptor ablation. *Molecular Therapy*. 2022;30(3):1315-1328. doi:10.1016/j.ymthe.2021.09.014
29. Chaffiol A, Caplette R, Jaillard C, et al. A New Promoter Allows Optogenetic Vision Restoration with Enhanced Sensitivity in Macaque Retina. *Mol Ther*. Nov 1 2017;25(11):2546-2560. doi:10.1016/j.ymthe.2017.07.011
30. Lee JW, Kim IT. Outcomes of idiopathic macular epiretinal membrane removal with and without internal limiting membrane peeling: A comparative study. *Japanese Journal of Ophthalmology*. 2010/03/01 2010;54(2):129-134. doi:10.1007/s10384-009-0778-0
31. Nukada K, Hangai M, Ooto S, Yoshikawa M, Yoshimura N. Tomographic features of macula after successful macular hole surgery. *Invest Ophthalmol Vis Sci*. Apr 1 2013;54(4):2417-2428. doi:10.1167/iovs.12-10838
32. La Heij EC, Dieudonné SC, Mooy CM, et al. Immunohistochemical Analysis of the Internal Limiting Membrane Peeled With Infracyanine Green. *American Journal of Ophthalmology*. 2005/12/01/ 2005;140(6):1123-1125. doi:https://doi.org/10.1016/j.ajo.2005.05.054
33. Zhang KY, Tuffy C, Mertz JL, et al. Role of the Internal Limiting Membrane in Structural Engraftment and Topographic Spacing of Transplanted Human Stem Cell-Derived Retinal Ganglion Cells. *Stem Cell Reports*. Jan 12 2021;16(1):149-167. doi:10.1016/j.stemcr.2020.12.001
34. Peynshaert K, Vanluchene H, De Clerck K, et al. ICG-mediated photodisruption of the inner limiting membrane enhances retinal drug delivery. *Journal of Controlled Release*. 2022/09/01/ 2022;349:315-326. doi:https://doi.org/10.1016/j.jconrel.2022.07.002

588 35. Janknecht P, Feltgen N, Wesendahl T, et al. Internal limiting membrane ablation in pig eyes with
589 the Er:YAG laser under perfluorodecalin. *Graefes Arch Clin Exp Ophthalmol*. Sep 2001;239(9):705-
590 711. doi:10.1007/s004170100343
591 36. Boye SE, Alexander JJ, Witherspoon CD, et al. Highly Efficient Delivery of Adeno-Associated Viral
592 Vectors to the Primate Retina. *Hum Gene Ther*. Aug 2016;27(8):580-597.
593 doi:10.1089/hum.2016.085
594 37. De Clerck K, Vanluchene H, Braeckmans K, De Smedt S, Remaut K, Peynshaert K. Characterization
595 of enhanced lipid nanoparticle delivery after photodisruption of the inner limiting membrane.
596 *Investigative Ophthalmology & Visual Science*. 2023;64(8):2614-2614.
597 38. Gandorfer A, Haritoglou C, Gass CA, Ulbig MW, Kampik A. Indocyanine green-assisted peeling of
598 the internal limiting membrane may cause retinal damage. *American Journal of Ophthalmology*.
599 2001/09/01/ 2001;132(3):431-433. doi:https://doi.org/10.1016/S0002-9394(01)01087-X

600

601

602

603 # Figure Legends

604 **Figure 1: Overview of study**

605 **A.** Following a pars plana vitrectomy, the ILM is stained with brilliant blue dye. **B.** Mechanical
606 force lifts the ILM in a circular pattern around the fovea using forceps. **C.** Intravitreal injection
607 delivers viral vector to the retina. **D.** A blue autofluorescence (BAF) confocal scanning laser
608 ophthalmoscope (cSLO) confirmed the presence of GCaMP in a pattern matching the surgical
609 peel two months post injection. **E.** Functional assessments were conducted at retinal imaging
610 locations using a blue 488nm excitation source in combination with a red LED flashing stimulus.
611 **F.** Individual RGCs were segmented and **G.** their responses to the LED stimulus tabulated.

612 **Figure 2: ILM Peeling enables AAV-mediated fluorescence beyond the fovea in macaque**

613 **A.** 30°cSLO BAF images centered on the fovea, taken in each eye of M1 including the A control
614 eye OS and **B.** the ILM peeled eye OD. GCAMP Fluorescence intensity contour (visualized in
615 lower panel, line denoted by white dashed line) is normalized to max value and smoothed.

616 AOSLO Imaging locations are labeled for each eye. **C.** Box plot of individual RGC Z-scores at
617 each imaging location, grouped by retinal eccentricity. Group responses are 12.7 ± 10.4, n=67;
618 10.0 ± 6.6, n=62; 11.52 ± 7.5, n = 85; 10.9 ± 7.6; n = 73; 6.4 ± 3.9, n=40, respectively. Taken at
619 17 weeks post intravitreal injection in OS and 21 weeks OD.

620 **Figure 3: RGC remain responsive for at least 6 months after ILM peel**

621 **A**. AOSLO GCaMP time-integrated image used to create segmentation masks at the edge of the
622 ILM peeled area at 9° from the fovea of M1 OD. **B.** Responses at two (6.7 ± 5.7, n=27), three
623 (6.0 ± 5.2, n=28), and five (6.4 ± 4.0, n=40) months post intravitreal injection, or three, four-,
624 and six-months post ILM peel. **C.** AOSLO GCaMP image within the ILM peeled area at 3.5° from
625 the fovea of M1 OD. **D.** Responses at three (8.9 ± 6.2, n=59), four (7.8 ± 6.6, n=68), five (12.5 ±
626 10.2, n=87), and six (11.5 ± 7.5, n=76) months post intravitreal injection. **E.** AOSLO GCaMP
627 image of the non-peeled eye at 3.5° from the fovea of M1 OS. **F.** Responses at one (6.7 ± 3.5,
628 n=97), two (6.3 ± 3.2, n=74), three (8.2 ± 2.9, n=81), and four (10.7 ± 6.0, n=75) months post
629 intravitreal injection.

630 **Figure 4: RGC response amplitudes measured in all eyes**

631 **A.** (left) 30°cSLO BAF images centered on the fovea for all experimental eyes, imaging locations
632 shown with blue squares. (right) Individual RGC Z-scores in box plots for M2 OD (12.7 ±
633 10.4,n=67, 11.5 ± 7.5,n=85, and 6.4 ± 3.95,n=40) taken five months post IVT injection, **B.** M2
634 OS (5.4 ± 2.5,n=12, 4.4 ± 2.9,n=17, 5.2 ± 3.3,n=30, and 4.4 ± 3.0,n=24) taken three months
635 post IVT injection, **C.** M2 OD (7.3 ± 4.6,n=81, 7.1 ± 6.2,n=77, and 6.2 ± 3.7,n=48) taken five
636 months post IVT injection, **D.** M3 OS (7.1 ± 4.3,n=52, 4.2 ± 1.5,n=31, 4.2 ± 2.1,n=12, and 4.9 ±
637 3.6,n=20) taken five months post IVT injection, **E.** M3 OD (8.3 ± 6.4,n=92, and 7.1 ± 4.4,n=99)
638 taken six months post IVT injection.

639 **Figure 5: Optical readout of RGC activity from the retinal nerve fiber layer**

640 **A.** 30°cSLO BAF images centered on the fovea of M1 OD (ILM-peeled). **B.** AOSLO GCaMP
641 time-integrated image taken at the Nasal region shown in M1 OD. The green dotted line
642 represents an area-integration used to construct a temporal signal for these RNFL bundles **C.**
643 30°cSLO BAF images centered on the fovea of M1 OS (non-peeled). **D.** The orange dotted line
644 represents an area-integration used to construct a temporal signal for these RNFL bundles **E.**
645 RNFL area-integrated traces responding to an OFF-onset of the LED stimulus at 60s and 100s
646 (Z-Score responses 3.36 ± 0.02, and 1.45 ± 0.02, respectively), filtered using moving median
647 filter as previously described.

648 **Figure 6: Structural imaging reveals minor morphological changes following ILM peel**

649 **A** (left) 55° Color fundus images of all ILM peeled eyes centered on the fovea and taken two-
650 months post ILM peel. White arrows indicate areas consistent with concentric macular dark
651 spots. (Right) B-scan OCT of the foveal pit between 2-24 weeks post ILM peel procedure and 1-
652 142 days post intravitreal injection.

653 **Figure 7: Circular retinal defects correspond to absence of ganglion cell fluorescence**

654 **A.** AOSLO calcium image of two exemplary hypofluorescent areas in M3 OS. Dendrites are
655 visible in this region. **B.** Color fundus (top-left) and cSLO BAF (top-right) of M3 OS showing two
656 hypofluorescent areas that are investigated with OCT (bottom). **C.** Montaged fluorescence
657 AOSLO image reveals dimples in OCT correspond to the two areas in AOSLO. **D.** Color fundus
658 location with no macular dark spots but a hypofluorescent region in the cSLO BAF **E.** OCT, and
659 AOSLO of the hyperfluorescent region seen in D. **F.** Color fundus location with CMDS streaks but
660 no visible RNFL dimples in OCT or **G.** hypofluorescent RGC expression in AOSLO.

661

662

663 # Figures

664 ## Figure 1

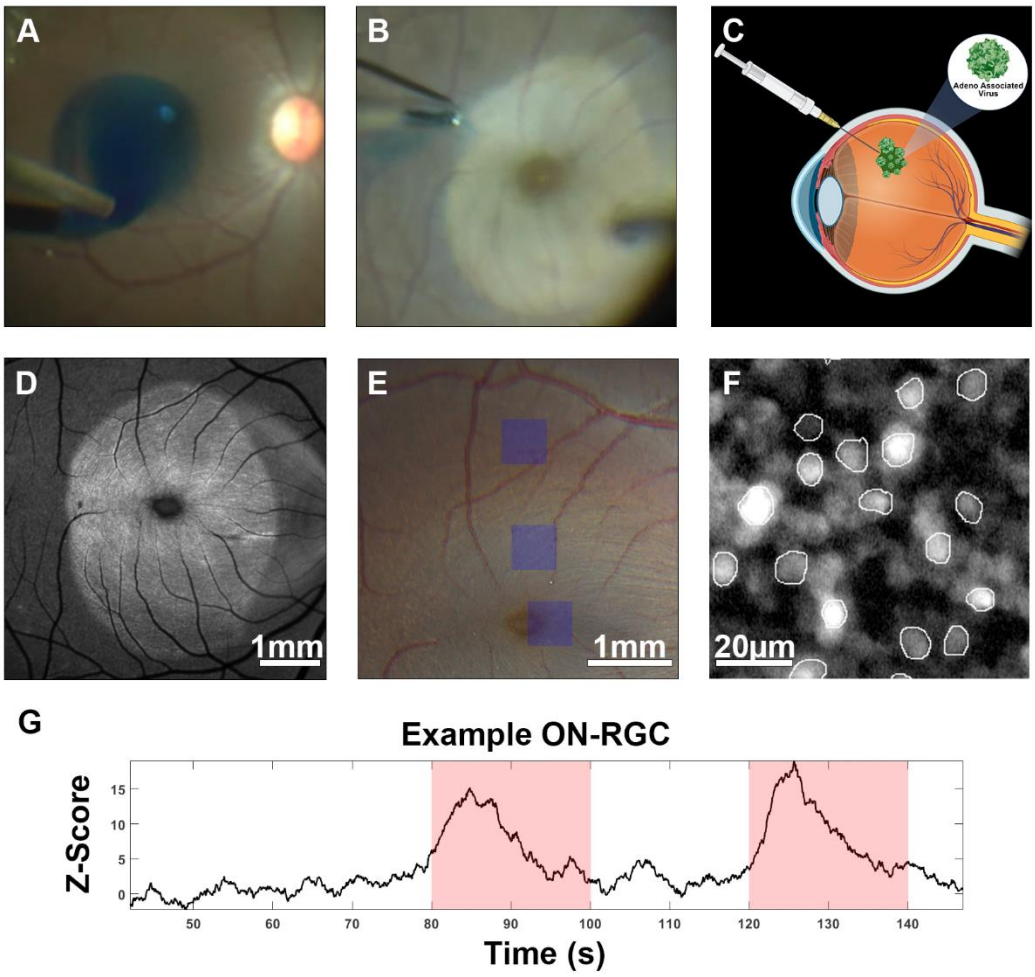

665

666

667

668

669

Figure 2

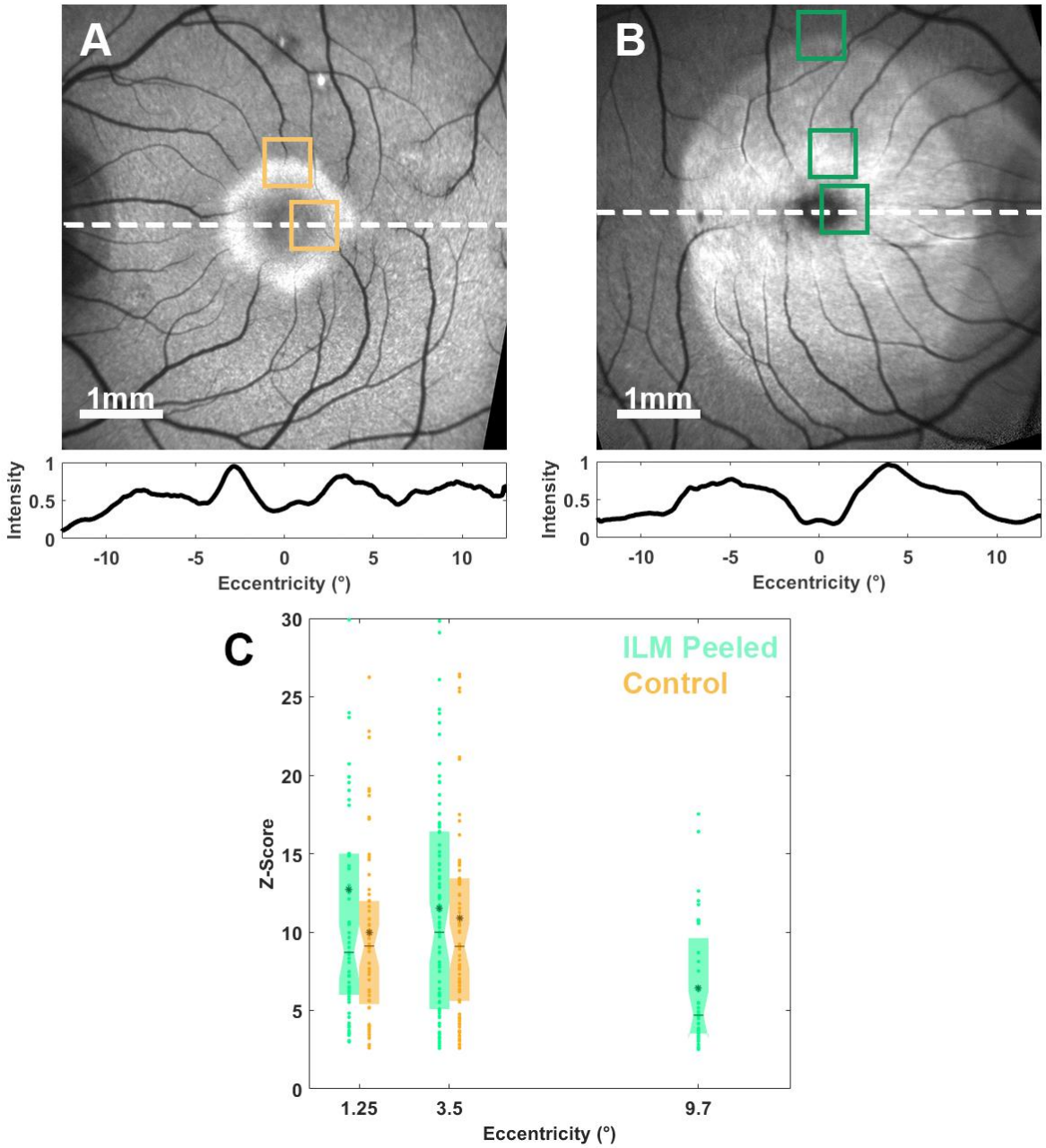
A
1mm
B
1mm
Intensity
1
0.5
0
-10
-5
0
5
10
Eccentricity (°)
C
ILM Peeled
Control
Z-Score
30
25
20
15
10
5
0
1.25
3.5
9.7
Eccentricity (°)

674 **Figure 3**

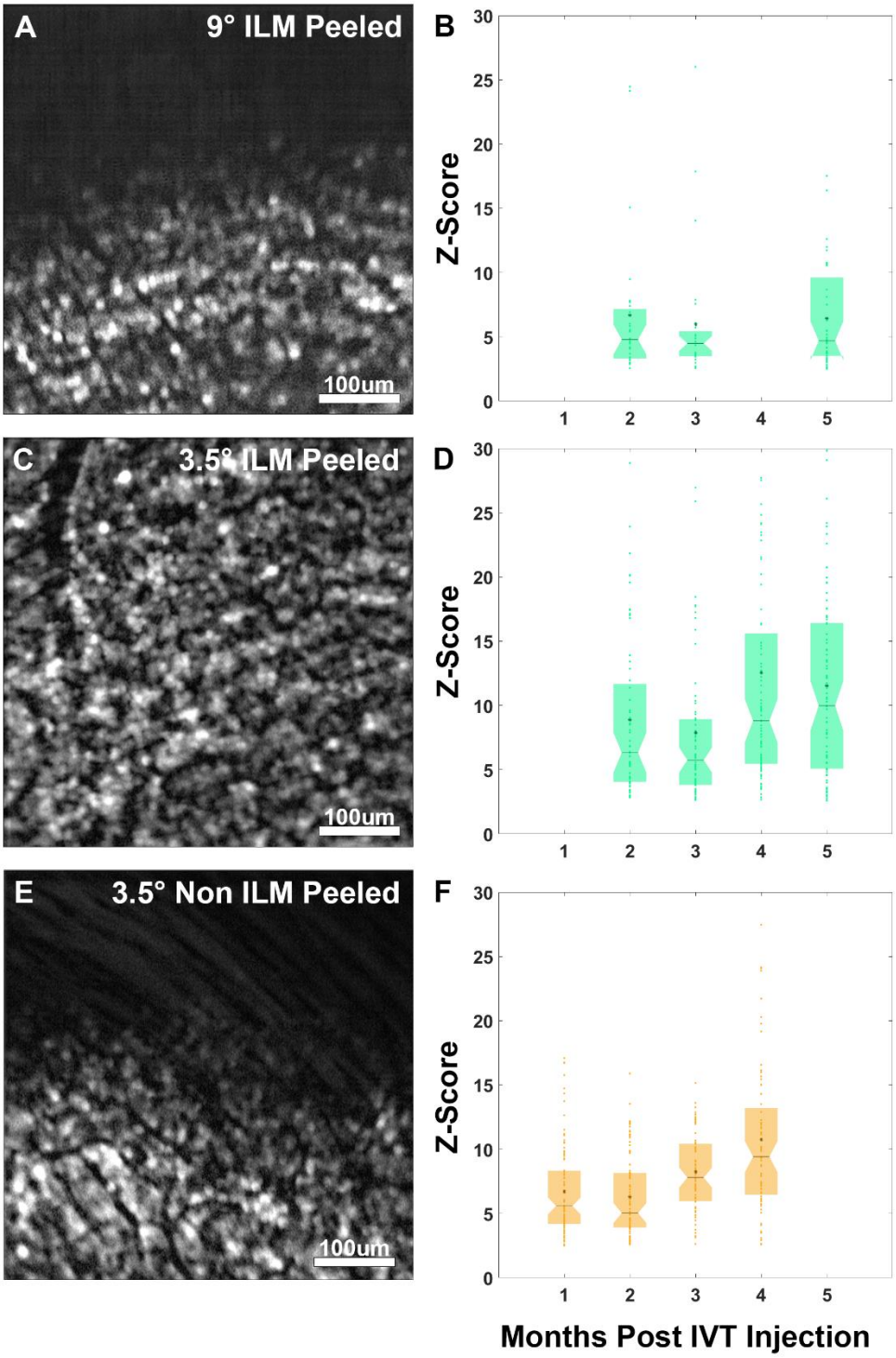

675

676 **Figure 4**

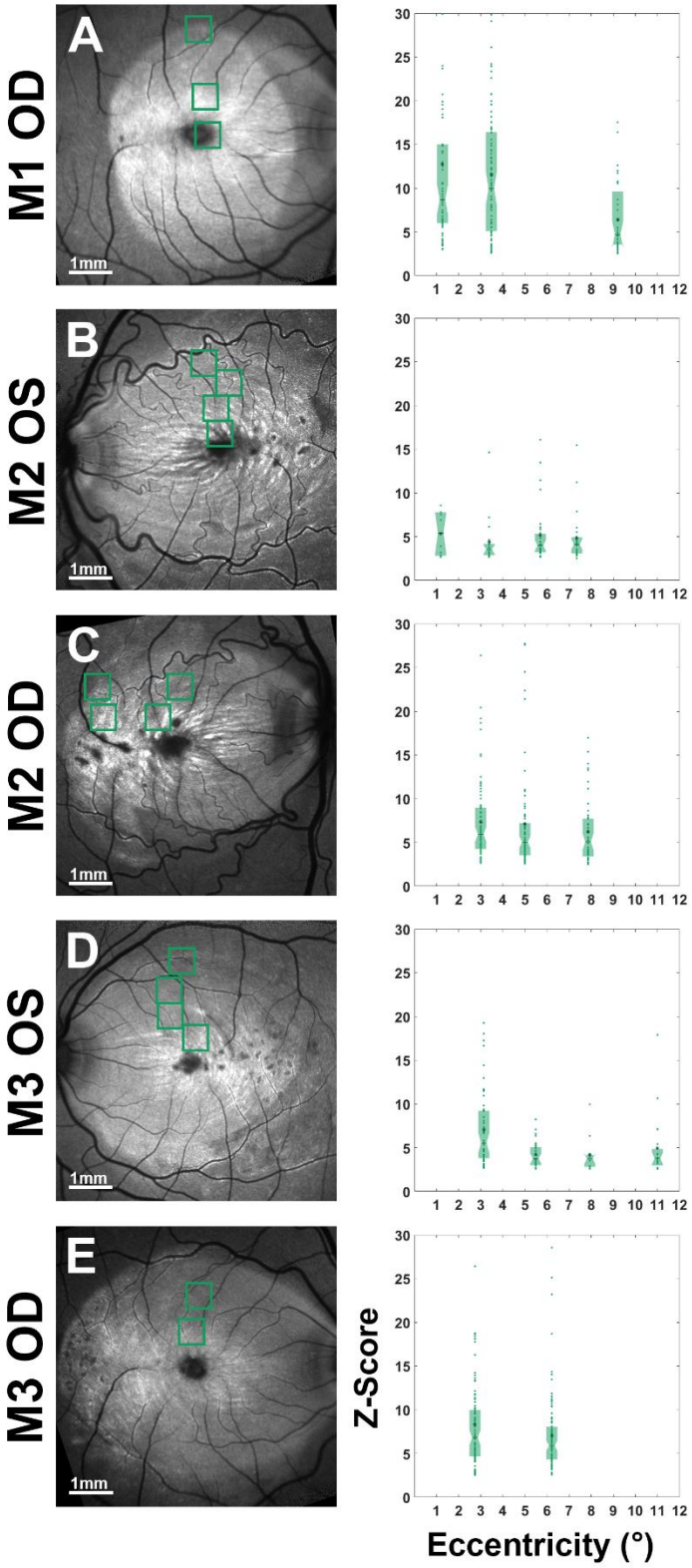

677

Figure 5

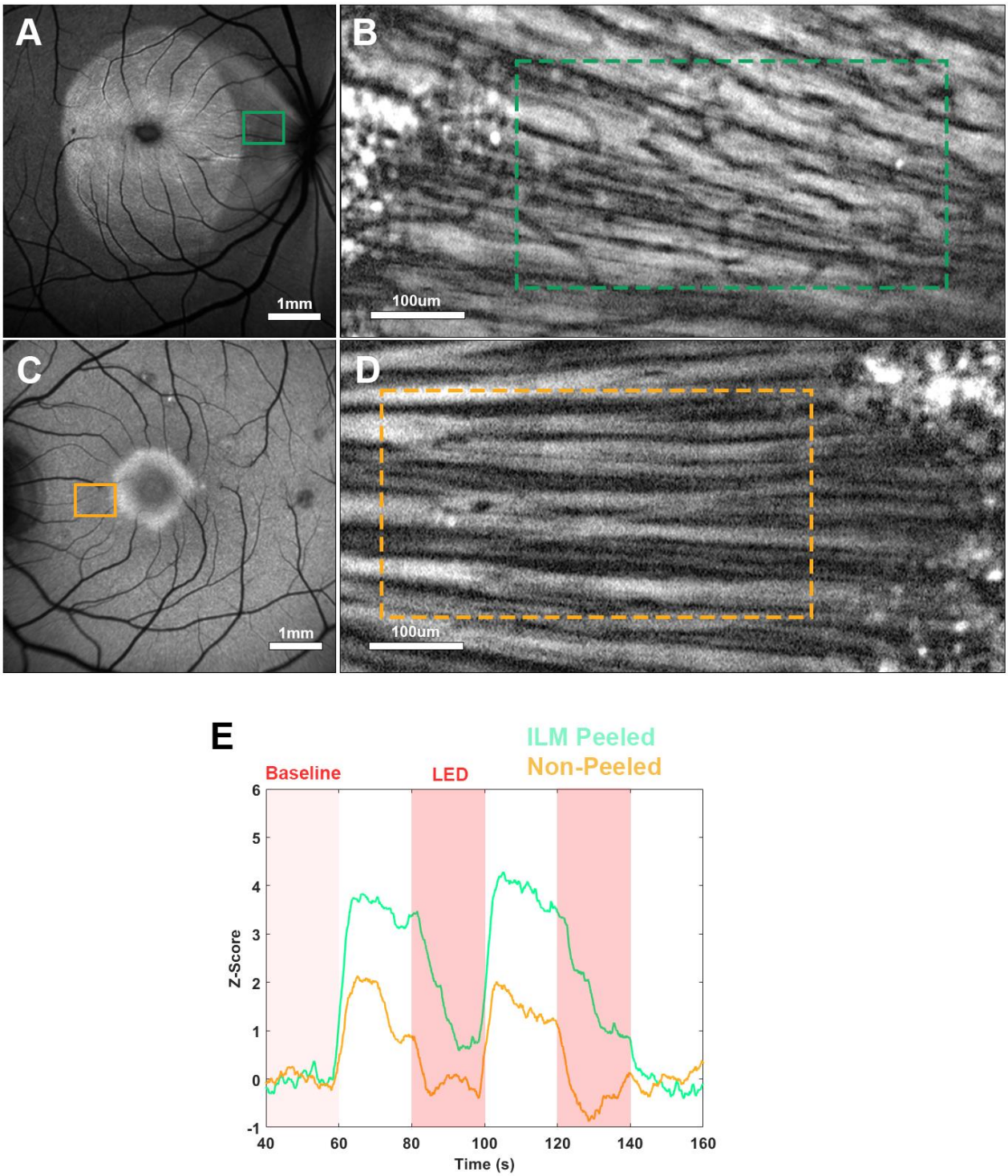
A
1mm
B
100um
C
1mm
D
100um
E
ILM Peeled
Non-Peeled
Baseline
LED
Z-Score
Time (s)
6
5
4
3
2
1
0
-1
40
60
80
100
120
140
160

681 **Figure 6**

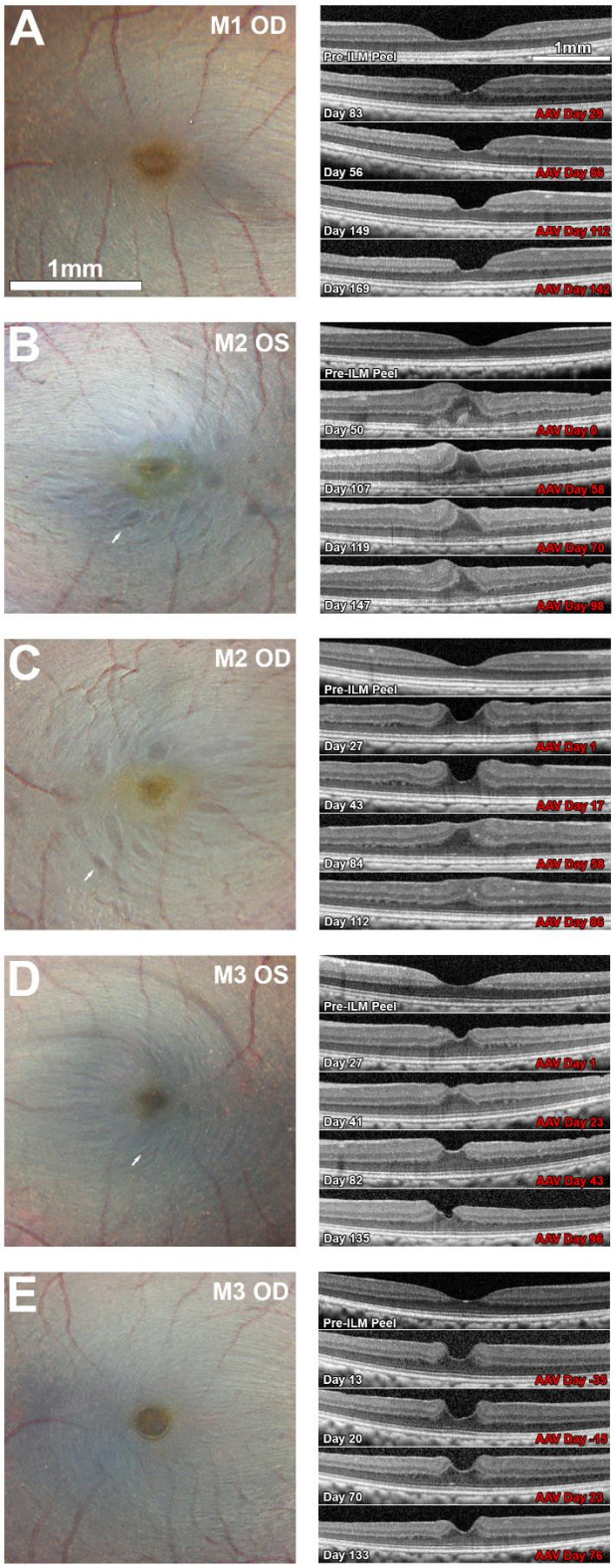

682

683 **Figure 7**

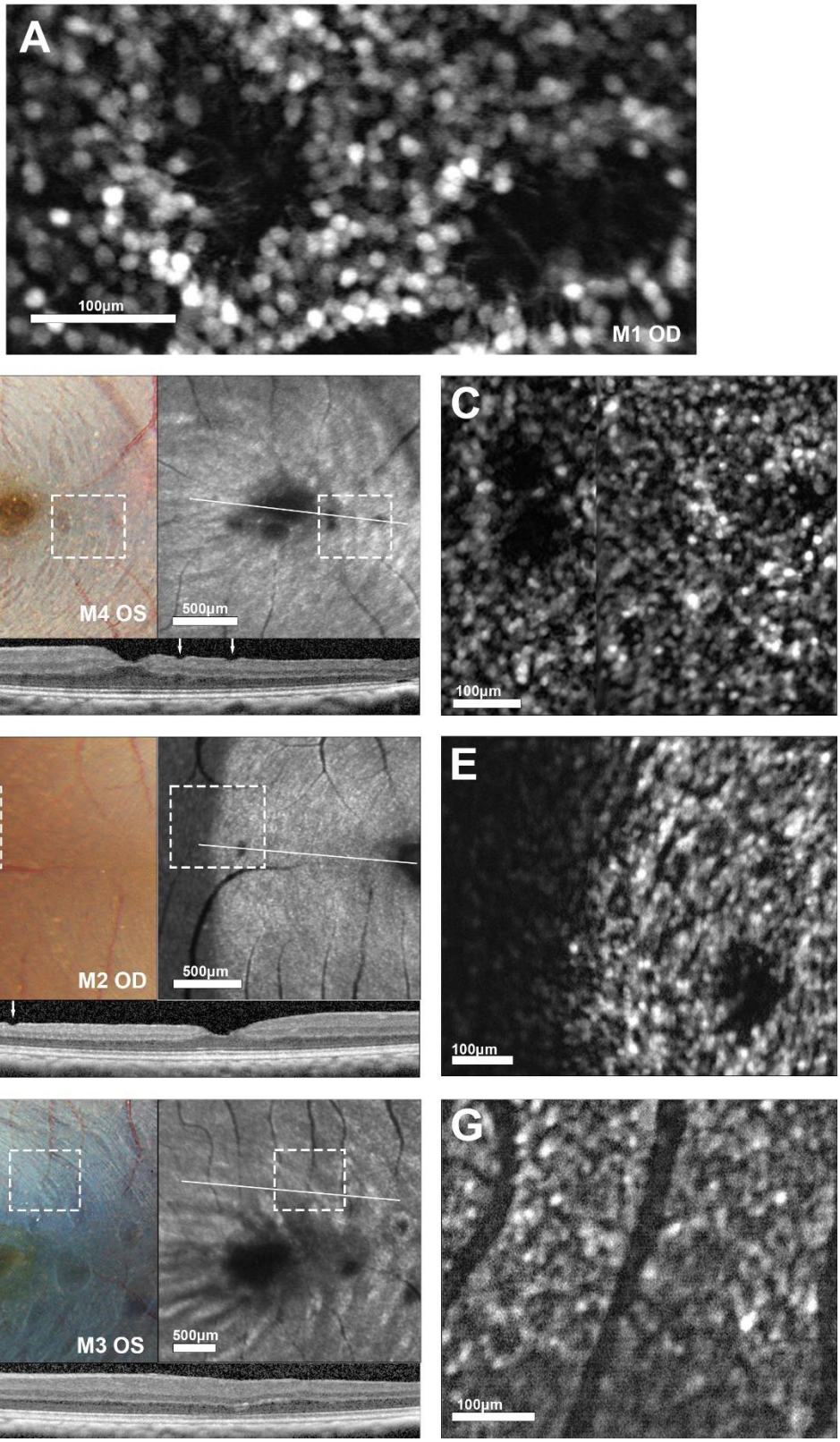

684

Tables

Table 1: Summary of demographic and experimental parameters for all eyes involved in the study.

The sex and age of the primate, immune suppression status quantity and type of viral vector injected intravitreally, and the time elapsing between the ILM peel and the intravitreal injection in days is listed for each eye.

Macaque (eye)	*sex*	Age at time of ILM peel	Inactivating antibodies to AAV2	Time between immune suppression and ILM peel (days)	Time between ILM peel and viral vector Injection (days)	Time of AAV2 injection after initial injection in fellow eye (days)	GCaMP Variant
M1 (OS)	*M*	Control	1:4	Control	Control	---	GCaMP8s
M1 (OD)		10y 9m		31	28	29	GCaMP8s
M2 (OS)	*M*	4y 2m	1:5	27	50	41	GCaMP8s
M2 (OD)		4y 3m		62	55	---	GCaMP8s
M3 (OS)	*F*	3y 10m	1:10	98	42	35	GCaMP8m
M3 (OD)		3y 11m		126	48	---	GCaMP8m

697 **Table 2: Ocular Inflammation scores**

698 Inflammation following intravitreal injection of the viral vector in all animals was scored
699 longitudinally by a masked board certified ophthalmologist based on a modified Hackett-
700 McDonald scoring system [16]. The assessment included slit lamp examination and observations of
701 pupillary response and dilation. Scores shown are integrated from the 9 numerical measures
702 listed in the attached Modified Hackett scoring sheet.

703

	Weeks post injection																
Animal	**-4**	**-3**	**-2**	**-1**	**0**	**1**	**2**	**3**	**4**	**5**	**6**	**7**	**8**	**9**	**10**	**11**	**12**
M2 OS							11		4		3	3	4		2		2
M2 OD	2		4			8	2		3		2					0	
M3 OS		2				0	4	4	2	3		2					
M3 OD	2					3	2	2		2							

704

705
706
707
708
709
710
711
712
713
714
715
716
717
718
719
720

721 # Supplementary Materials

722

723 Modified Hackett-McDonald Scale for Ocular Inflammation in NHPs

724

725

CONJUNCTIVA

Congestion

0 Normal. May appear blanched to reddish pink without perilimbal injection (except at 12:00 and 6:00 positions) with vessels of the palpebral and bulbar conjunctiva easily observed.

1+ A flushed reddish color predominantly confined to the bulbar conjunctiva with some perilimbal injection. Primarily confined to the lower and upper parts of the eye from the 4:00 and 7:00 and the 11:00 and 1:00 positions.

2+ Bright red color of the bulbar and palpebral conjunctiva with accompanying perilimbal injection converging at least 75% of the circumference of the perilimbal region.

3+ Dark, beefy red color with congestion of the bulbar and the palpebral conjunctiva along with pronounced perilimbal injection. Petechia may be present on the conjunctiva. The petechial generally predominate along the nictitating membrane and the upper palpebral conjunctiva.

Swelling

0 Normal or no swelling of the conjunctival tissue

1+ Swelling above normal without eversion of the lids (can be easily ascertained by noting that the upper and lower eyelids are positioned as in the normal eye); swelling generally starts in the lower cul-da-sac near the inner canthus, which requires slit lamp examination.

2+ Swelling with misalignment of the normal approximation of the lower and upper eyelids; primarily confined to the upper eyelid so that in the initial stages the misapproximation of the eyelids begins by partial eversion of the upper eyelid. In this stage, swelling is confined generally to the upper eyelid, although it exists in the lower cul-de-sac (observed best with the slit lamp).

3+ Swelling definite with partial eversion of the upper and lower eyelids essentially equivalent. This can be easily ascertained by looking at the animal head-on and noticing the positioning of the eyelids; if the eye margins do not meet, eversion has occurred.

4+ Eversion of the upper eyelid is pronounced with less pronounced eversion of the lower eyelid. It is difficult to retract the lids and observe the perilimbal region.

726

Discharge

0 No discharge (except as noted above).

1+ Discharge is above normal and present on the surface of the eye or in the medial canthus, but not on the lids of hairs of the eyelids.

2+ Discharge is abundant, easily observed, and has collected on the lids and around the hairs of the eyelids.

3+ Discharge has been flowing over the eyelids so as to wet the hairs substantially on the skin around the eyes.

CORNEA

Opacity

0 Normal cornea. Appears with the slit lamp as having a bright grey line on the epithelial surface and a bright grey line on the endothelial surface with a marble-like grey appearance of the stroma.

1+ Some loss of transparency. Only the epithelium and/or the anterior half of the stroma is involved as observed with an optical section of the slit lamp. With diffuse illumination, the underlying structures are clearly visible, although some cloudiness may be readily apparent.

2+ Some loss of transparency. The cloudiness extends past the anterior half of the stroma. The affected stroma has lost its marble-like appearance and is homogeneously white. With diffuse illumination, underlying structures are visible, although there may be some loss of detail.

3+ Involvement of the entire thickness of the stroma. With optical section, the endothelial surface is still visible. However, with diffuse illumination, the underlying structures are just barely visible (to the extent that the observer is still able to grade flare, iris vessel congestion, observe for pupillary response, and note lenticular changes).

4+ Involvement of the entire thickness of the stroma. With optical section, the endothelium is not clearly visualized. With diffuse illumination, the underlying structures cannot be seen so that the evaluation of aqueous flare, iris vessel congestion, pupillary response, and lenticular changes is not possible.

% Area of Opacity

0 Normal cornea with no area of cloudiness

1 1 to 25% area of stromal cloudiness

2 26 to 50% area of stromal cloudiness

3 51 to 75% area of stromal cloudiness

4 76 to 100% area of stromal cloudiness

Vascularization

0 No corneal vascularization (pannus)

1 Vascularization is present but vessels have not invaded the entire corneal circumference. Where localized vessel invasion has occurred, they have not penetrated beyond 2 mm.

2 Vessel invasion is greater than 2 mm in one of more areas, or involves the entire corneal circumference.

AQUEOUS

Flare

0 No protein is visible in the anterior chamber when viewed by an experienced observer using slit lamp biomicroscopy.

Trace Trace amount of protein is detectable in the anterior chamber. This protein is only visible with careful scrutiny by an experienced observer using slit lamp biomicroscopy.

1+ Mild amount of protein is detectable in the anterior chamber. The presence of protein in the anterior chamber is immediately apparent to an experienced observer using slit lamp biomicroscopy.

2+ Moderate amount of protein is detectable in the anterior chamber. These grades are similar to 1+ but the opacity would be readily visible to the naked eye of an observer using any source of a focused beam of white light. This is a continuum of moderate opacification with 2+ being less apparent than 3+.

3+ Moderate amount of protein is detectable in the anterior chamber. These grades are similar to 1+ but the opacity would be readily visible to the naked eye of an observer using any source of a focused beam of white light. This is a continuum of moderate opacification with 3+ being more apparent than 2+.

4+ Large (severe) amount of protein is detectable in the anterior chamber. Similar to 3+ but the density of the protein approaches that of the lens. Additionally, frank fibrin deposition is frequently seen in acute circumstances. It needs to be noted that because fibrin may persist of a period of time after partial or complete restoration of the blood-aqueous barrier, it is possible to have resorbing fibrin present with lower numeric assignations for flare (e.g., 1+ flare with fibrin).

Cell

0 No cells are seen in a single field of the focused slit lamp beam. No cells are visualized as the slit lamp beam is swept across the anterior chamber.

Trace Rare (1-5) cells are seen in a single field of the focused slity lamp beam. When the instrument is held stationary, not every optical section contains circulating cells.

1+ 6-25 cells are seen in a single field of the focused slit lamp beam. When the instrument is held stationary, each optical section of the anterior chamber contains circulating cells.

2+ 26-50 cells are seen in a single field of the focused slit lamp beam. When the instrument is held stationary, each optical section of the anterior chamber contains circulating cells.

3+ 51-100 cells are seen in a single field of the focused slit lamp beam. When the instrument is held stationary, each optical section of the anterior chamber contains circulating cells. Keratic precipitates or cellular deposits on the anterior lens capsule may be present.

4+ Greater than 100 cells are seen in a single field of the focused slit lamp beam. When the instrument is held stationary, each optical section of the anterior chamber contains circulating cells. Keratic precipitates or cellular deposits on the anterior lens capsule may be present. As for fibrin deposition, hypopyon or clumps of cells may persist for some period of time after the active exudation of cells into the anterior chamber has diminished or ceased entirely. Thus, it is possible to have resorbing hypopyon present with lower numeric assignations for cell (e.g., 1+ cell with hypopyon).

<u>OTHER</u>

Iris Congestion

0 Normal iris without any hyperemia of the iris vessels. Occasionally around 12:00 to 1:00 position near the pupillary border and the 6:00 and 7:00 position near the pupillary border there is a small area, about 1 to 3 mm in diameter, in which the secondary and tertiary vessels are slightly hyperemic.

1+ Minimal injection of secondary vessels but not tertiary. Generally, it is uniform, but may be of greater intensity at the 12:00 or 6:00 position. If it is confined to the 12:00 or 6:00 position, the tertiary vessels mush be substantially hyperemic.

2+ Minimal injection of the tertiary vessels and minimal to moderate injection of the secondary vessels.

3+ Moderate injection of the secondary and tertiary vessels with a slight swelling of the iris stroma (this gives the iris surface a slightly rugose appearance, which is usually most prominent near the 3:00 and 9:00 positions).

4+ Marked injection of the secondary and tertiary vessels with marked swelling of the iris stroma. The iris appears rugose; may be accompanied by hemorrhage (hyphemia) in the anterior chamber.

Lens Opacity

Incomplete A diffuse lens opacity visible upon gross inspection of the eye with an indirect ophthalmoscope or other focal light source and retroillumination. The view of the fundus is significantly impaired but a red-reflex can still be obtained. Upon slit lamp biomicroscopy the opacity involves multiple regions of the lens.

Complete A diffuse lens opacity visible upon gross inspection of the eye with an indirect ophthalmoscope of other focal light source. The fundus cannot be seen and a red-reflex cannot be elicited. Upon slit lamp biomicroscopy, the entire lens is opaque.

Resorbing A diffuse lens opacity visible upon gross inspection of the eye with an indirect ophthalmoscope of other focal light source. The fundus may or may not be visible and a red-reflex may or may not be elicited. The lens capsule may be wrinkled and the lens itself is dehydrated and flattened or liquid and soft in appearance. Upon slit lamp biomicroscopy the entire lens in involved in the opacity.

Punctate A focal or multifocal, discrete, dot-like lens opacity that is visible only to a trained observer with a SL-14 slit lamp biomicroscope at high magnification.

Incipient A focal lens opacity that is visible upon gross inspection of the eye with an indirect ophthalmoscope of other focal light source and retroillumination. The view of the fundus is minimally impaired by the opacity. Upon slit lamp biomicroscopy the opacity can be localized to a specific regions of the lens and other regions of the lens appear normal.